

Synthesis and Characterization of Nanocomposite-Based Heteropolyacid, and its Catalytic, Photocatalytic and Electrochemical Performances

H. Salavati^{1,*}, A. Teimouri¹, S. Kazemi²

¹ Chemistry Department, Payame Noor University, 19395-3697, Tehran, Iran

² Department of Chemistry, Faculty of Science, University of Birjand, P. O. Box 97175-615, Birjand, Iran.

*E-mail: hosseinsalavati@pnu.ac.ir

Received: 29 August 2017 / Accepted: 25 December 2017 / Published: 5 February 2018

This work reports the synthesis and characterization as well as catalytic, photocatalytic and electrochemical performances of a novel supported catalyst based on $\text{H}_5\text{PMo}_{10}\text{V}_2\text{O}_{40}$ Keggin type polyoxometalate (PMoV) immobilized on melamine grafted graphene oxide (Mel-GO). The supported catalyst (PMoV@Mel-GO) was characterized by X-ray diffraction spectroscopy (XRD), field emission scanning electron microscopy (FESEM), furrier transforms infrared spectroscopy (FT-IR), cyclic voltammetry (CV) and UV-vis diffuse reflectance spectroscopy (UV-DRS). Electrochemical characterizations revealed that modified graphene oxide nano-sheets have excellent photocatalytic activity towards electron transfer. Electrochemical impedance spectroscopy (EIS) and cyclic voltammetry (CV) spectroscopy confirmed the role of Keggin type polyoxometalate in charge transfer and electron transfer changes. The electroactive surface areas of the pure CPE and catalyst/CPE were appraised by CV technique confirming that for supported catalyst, modified electrode is approximately greater than that for pure CPE. For the optimization of main factors in photocatalytic activity, a statistical method called response surface methodology (RSM) based on the central composite design (CCD) was used to economize on the number of experiments and their meaningful interpretations. The supported catalyst showed high photocatalytic activity and reusability in the degradation of methylene blue (denoted as MB) as pollutant. Optimization results for initial dye concentration 20 mg/L showed that maximum degradation efficiency, 97.71%, was achieved at optimum conditions, catalyst amount 17.5 mg and pH= 6.1 for reaction time 66 min. In addition, the catalyst showed high activity in the desulfurization of dibenzothiophene (abbreviated as DBT) to dibenzothiophene sulfone product (denoted as DBTO₂) using formal batch method with 98.2% conversion at 50°C. In addition, the sulfone product was characterized by NMR, FT-IR, Mass spectroscopy and GC analysis. The optimal conditions for conversion of DBT were found to be; H_2O_2 / DBT3:1, reaction temperature 50 °C and reaction time 120 min for 0.05 g catalyst amount.

Keywords: Cyclic Voltammetry, Electrochemical, Graphene oxide, Heteropolyacid, Photocatalytic

1. INTRODUCTION

What has resulted in polyoxometalates' different applications in the field of medicine, surface chemistry, photochemistry, and electrochemistry is their versatility and accessibility. Furthermore, among different structures of polyoxometalates participating in photocatalysts, Keggin type heteropolyacid is of particular importance because of its high chemical and mechanical resistance under reaction conditions; moreover, the lowest vacant d molecular orbital in octahedral (MO_6) of this structure is nonbonding and metal-centered causing its reversible reduction to form a multi-valance species [1-7]. The immobilization of polyoxometalates on electrodes surface makes their electrochemical study and applications easy. polyoxometalates can be immobilized on electrode surfaces by various methods such as immobilization, which serves as a dopant in conductive polymeric matrices, modification, layer-by-layer approaches, adsorption and immobilization in inorganic matrices. Among these methods, entrapment of POMs into inorganic matrices was investigated as an attractive methodology for sensor fabrication due to its simplicity and stability [8-12]. One of the solid supports with unique properties is graphene oxide (GO) that has a layered structure, characterized by functional groups on surfaces like epoxide, carboxyl and hydroxyl. GO shows extraordinary characteristic properties such as exceptional thermal properties and strong mechanical strength, high ratio of surface area ($2630 \text{ m}^2/\text{g}$), etc. [13]. GO nano-sheets have hydrophilic properties because of the wide range of functional groups containing oxygen on the surface of layers of graphene oxide nano-sheets [14,15]. To provide great potential for applications in different sciences [16-25], different surfactants, nanoparticles and polymeric materials easily functionalize graphene oxide nano-sheets.

Desulfurization of model oil has become an environmentally important phenomenon worldwide. Compared to traditional hydro-desulfurization method (HDS), oxidative desulfurization (ODS) is more efficient for this purpose because it needs no harsh conditions such as gaseous hydrogen, high pressure and temperature. Recently, various investigators have found that the pyrolysis of graphene oxide with a low-cost N source such as melamine and urea [26-28] is a versatile process for large-scale production of graphene oxide nano-sheets with flexible control over the N bonding configuration. It has been found that the nature of N functionalities in the resulting graphene oxide nano-sheets is largely determined by the structure of N source and the pyrolysis temperature. It should be noted that the nitrogen atoms in the $-\text{NH}_2$ bonds can also offer lone pairs of electrons, which effectively attract metallic cations. Therefore, nitrogen-containing groups have been widely used for complexing metal ions [29]. Accordingly, amination of GO is expected to improve its capability for linkage of cation ions [30-32]. Many investigations have been performed to prepare nitrogen-doped graphene for consideration of catalytic, photocatalytic and electro-catalytic applications [33-41]. Thereupon, the main aim of the present study is to consider a novel system for photocatalytic properties by using Keggin type polyoxometalate immobilized over graphene oxide modified with melamine as natural molecule. As an advantage of this catalyst, the high surface area of the graphene oxide support can be combined to immobilize catalytic active molecules as heterogeneous catalysts with the melamine as a carrier of functional $-\text{NH}_2$ groups to connect to polyoxometalate and to create the active sites. In addition, we describe the photocatalytic activity of the catalyst and photo-degradation by visible light irradiation of dyes as pollutants using a synthesized photo-catalyst with

GO and melamine as environmentally friendly elements and Keggin type polyoxometalate because of its vacant d orbitals for exciting the electron for electron transfer reactions. In addition, cyclic voltammetry and impedance spectroscopy were applied for the investigation of electrochemical behaviors.

2. EXPERIMENTAL

2.1. Materials and methods

We obtained solvents, reagents and chemicals from chemical companies such as Merck, Fluka and Aldrich; and the samples were ground into a fine powder for characterization. FT-IR spectra were obtained as potassium bromide pellets in the range of 400-4000 cm^{-1} with a Nicolet-Impact 400D instrument. Field emission scanning electron microscopy (FESEM) of the catalysts and supports were taken on SEM Philips XL 30 instrument. Diffuse reflectance spectroscopy (DRS) was recorded on a 160 Shimadzu spectrophotometer, and X-ray diffraction (XRD) patterns were recorded with a Philips X-ray diffractometer (Model PW1840). Cyclic voltammetry (CV) was taken on Metrohm (model 797 VA) Processor instrument, and the reaction products were identified by GC-MS. NMR spectra were recorded in CDCl_3 on a Bruker 250 MHz spectrometer, and the mass spectra were recorded by the GSMS-QP 5050 Shimadzu.

2.2. Photocatalytic activity

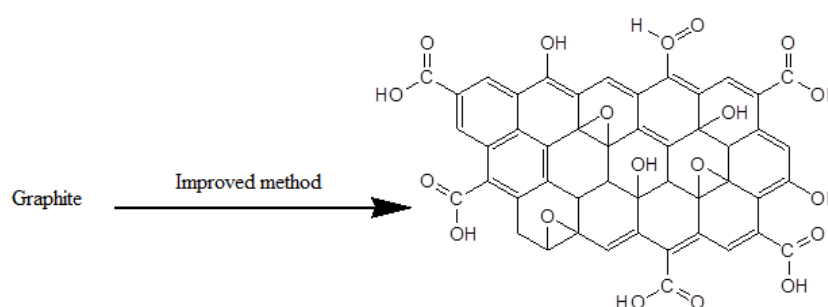
With regard to the fact that heterogenization of homogeneous catalyst is incredibly interesting because it can be recovered, we decided to immobilize PMoV on modified graphene oxide nano-sheets, and investigate its photocatalytic activity in the degradation of methylene blue as a pollutant.

2.3. Catalytic activity test for oxidation of DBT

DBT was oxidized to the corresponding sulfone by stirring a solution of the sulfide (1 mmol) and the catalyst (0.05 g) in n-octane/acetonitrile (w/w 2:1). The catalytic activity of oxidation of dibenzothiophene was investigated using acetonitrile as an extracting agent. After that, a certain quantity of H_2O_2 (30% aq.) was added as a green environmentally friendly oxidant. The mixture was placed under stirring for a specified time at 50°C, and thin-layer chromatography was employed to monitor the reaction. When the reaction was completed, centrifugation was used to separate the catalyst from the reaction solution. GC analysis of the oil phase showed that during oxidative desulfurization of DBT, the DBT was reduced; while no peaks attributed to sulfoxide and sulfone were observed. The absence of DBTO_2 and DBTO in oil phase confirmed that sulfone was extracted into a solvent phase. By evaporating the acetonitrile solvent at room temperature, a solid crystal product was obtained; and it was characterized by various methods such as NMR, FT-IR, and mass and GC analysis.

2.4. Preparation of graphene oxide (denoted as GO)

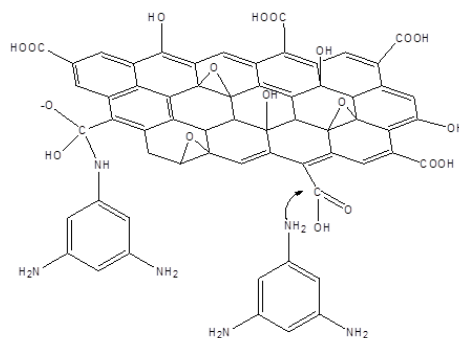
For the improved method, a 9:1 mixture of concentrated $\text{H}_2\text{SO}_4/\text{H}_3\text{PO}_4$ (360:40 mL) was added to a mixture of graphite powder (3.0 g, 1 wt equiv), and then KMnO_4 (18.0 g, 6 wt equiv) was slowly added to the resultant mixture producing a slight exotherm to 35-40°C. The mixture was then heated to 50°C and stirred for 12 h; then, it was cooled to room temperature and was poured onto ice (400 mL) with 30% H_2O_2 (3 mL). The mixture was centrifuged (4000 rpm for 4 h), and the supernatant was decanted away. Then, the remaining solid material was washed with 200 mL of water, 200 mL of 30% HCl , and 200 mL of ethanol prior to being centrifuged under 4000 rpm for 4 h before the supernatant was decanted away. After this extended multiple-wash process, the remaining material was coagulated with 200 ml of ether. Then, the resulting suspension was filtered over a PTFE membrane with a 0.45 pore size. The solid remaining on the filter was vacuum-dried overnight at room temperature, and 5.8 g of product was obtained [42]. Scheme 1 shows the structure of the resultant graphene oxide.



Scheme 1. Structure of synthesized graphene oxide

2.5. Preparation of melamine-grafted graphene oxide (denoted as melamine-GO)

A melamine covalently modified graphene oxide was prepared. Briefly, a suspension of graphene oxide in DMF solvent (7.5: 15 mg / mL) was prepared (solution 1), then a melamine solution in DMSO (5: 1 mg / mL) was prepared (solution 2); finally, the suspension of graphene oxide was mixed with dispersion of melamine. The material was stirred and heated for 24 h at 100°C. The melamine was grafted to GO via a covalent interaction between carboxyl groups and amine groups that were present in the GO solution. Moreover, the hydrogen bonding between the amine group in melamine and groups containing oxygen in GO and π - π interaction between the GO and triazine ring of melamine could also happen [44]. It should be noted the electrostatic interactions are possible between positive charge of amine groups in melamine and negative charge of carboxylic groups in graphene oxide.

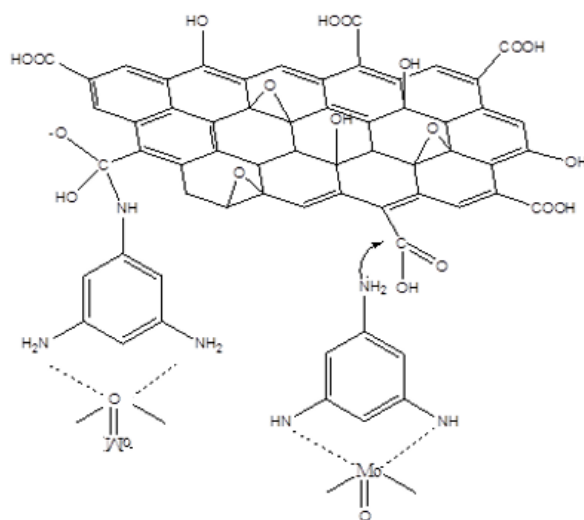


Scheme 2. Structure of synthesized melamine grafted graphene oxide

2.6. Preparation of kegglin type polyoxometalate (PMoV)

Keggin type polyoxometalate (denoted as PMoV) was synthesized by previously reported technique [43]. To describe it briefly, 18.0 g of $\text{Na}_2\text{HPO}_4 \cdot 12\text{H}_2\text{O}$ was dissolved in 250 ml distilled water, and 11.5 g of V_2O_5 was dissolved in 100 ml of 2 mol/L Na_2CO_3 solution. After that, they were mixed and heated until they boiled. After thirty minutes, a 400 ml solution containing 121.0 g of $\text{Na}_2\text{MoO}_4 \cdot 2\text{H}_2\text{O}$ was introduced into the above solution keeping the temperature at 90°C for 30 min. Then, 1:1 H_2SO_4 was added (dropwise and while being stirred) to the solution until $\text{pH}=2$. The mixture was cooled to room temperature while being stirred, and 50 ml ether was also added to it.

2.7. Preparation of supported catalyst with Keggin type polyoxometalate (denoted as PMoV @Mel-GO)



Scheme 3. Proposed schemes for linkage of PMoV on the surface of modified graphene oxide

The supported catalyst was synthesized by ultrasonic irradiation method. In this way, 0.2 g melamine-GO was dispersed in ethanol under ultrasonic irradiation for 30 min (solution 1). After that,

a solution of PMoV was prepared in ethanol by dispersing 0.05 g PMoV (solution 2), then solution 2 was added to solution 1 under ultrasonic irradiation for 45 min. This mixture was stirred for 12 h under magnetic stirring, and after that, it was centrifuged and dried at 60°C. Scheme 3 shows the structure of synthesized supported catalyst.

3. RESULTS AND DISCUSSION

3.1. Sample characterization

FTIR spectra are a vital tool to characterize both covalent and non-covalent functionalization of graphene oxide nano-sheets. The FT-IR spectrum of pristine graphite showed the characteristic band at 3430 cm^{-1} for O-H stretching and at 1640 cm^{-1} for skeletal vibrations from graphitic domains of adsorbed water and aromatic domain (C=C), respectively (Fig. 1a). Fig. 1b shows the FT-IR spectra of prepared graphene oxide; and the following functional groups were identified in graphene oxide: (3300-3400 cm^{-1}) related to O-H stretching vibrations, (1720-1740 cm^{-1}) subjected to C=O stretching vibration. Characteristic bands for C=C from unoxidized sp^2 C-C bonds appeared in (1590-1621 cm^{-1}), and C-O vibrations appeared at 1228 cm^{-1} and, for epoxide groups, at (849, 1048 cm^{-1}) ranges [42]. The characteristic bands for melamine are observed at 3470 cm^{-1} , 3418 cm^{-1} , 3328 cm^{-1} related to stretching vibration of triazine groups in melamine, and a band at 810 cm^{-1} corresponds to the stretching vibration of N-H group, which is a characteristic peak for melamine backbone (Fig. 1c). Some new peaks at 1732 cm^{-1} for C-O stretching appeared for graphene oxide, 3460 cm^{-1} for O-H stretching, and 1044 cm^{-1} and for C-O stretching from that of pristine graphite. After melamine was grafted to graphene oxide, the peak at (1720-1740 cm^{-1}) regions subjected to C=O stretching vibration disappeared due to the covalent bonding between melamine and carboxylic groups of graphene oxide (Fig. 1d). The peak related to C=C group shows a shift to 1628 cm^{-1} , and the epoxide stretching vibration of GO at 1044.32 cm^{-1} has shifted to 1044.38 cm^{-1} indicating H-bonding between melamine and hydroxyl group of GO. The hydrogen bonding between the amine group in melamine and groups containing oxygen in GO and π - π interaction between the GO and triazine ring of melamine can also happen. The increased frequency of vibration is due to the ring structure of H-bonded hydroxyl group of GO in the GO-Mel nano-composite [42, 43]. In addition, the peak at 810 cm^{-1} for triazine ring in melamine [44] shifted to 808 because melamine grafted covalently to graphene oxide (Fig. 1d). FT-IR spectrum of the Keggin type polyoxometalate (PMoV) showed absorption bands at 1059, 961, 842 and 775 cm^{-1} , corresponding to the four typical skeletal vibrations of the Keggin type polyoxoanion (Fig. 1e). FT-IR spectrum of the prepared catalyst showed absorption bands at 1046, 950, 833 and 770 cm^{-1} , corresponding to the four typical skeletal vibrations of the Keggin type polyoxoanion [44], with the shift due to the immobilization of Keggin type polyoxometalate on the surface of modified graphene oxide. This indicated that PMoV was supported on Mel-GO (Fig. 1f). These peaks could be attributed to ν (P=O_a), ν (Mo=O_t), ν (Mo-O_b-Mo) and ν (Mo-O_c-Mo), (O_t= terminal oxygen, O_b = bridged oxygen of two octahedral sharing a corner and O_c = bridged oxygen sharing an edge). Moreover, the peak is related to free amino group of melamine, which appeared at 808. It disappeared after supporting polyoxometalate confirming that the Keggin type polyoxometalate was covalently linked to modified graphene oxide (Fig. 1f). On the other hand, the narrow peak at 3470 cm^{-1} originating from

N-H bond in melamine changes to a broad peak around 3405 cm^{-1} in the supported catalyst [45]. Moreover, two broad peaks at around 2690 cm^{-1} and 2850 cm^{-1} appear in the supported catalyst. Note that there also appear 1118 , 1163 , 1207 and 1352 cm^{-1} peaks in the supported catalyst, which can be probably attributed to C-NH-C units and is another evidence for the forming of melam [46, 47].

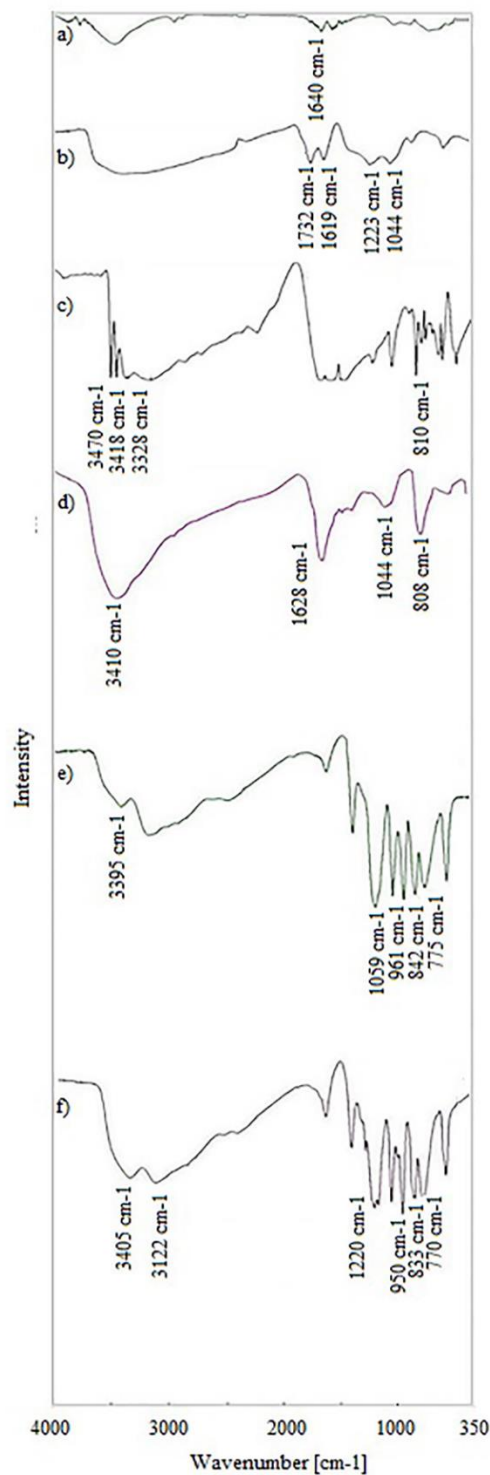


Figure 1. FTIR spectrum of a) graphite b) GO, c) melamine, d) Mel-GO, e) PMoV, f) PMoV@ Mel-GO

UV-DR spectra of GO, melamine, PMoV, Mel-GO and PMoV@Mel-GO were studied. The UV spectra of GO showed absorption bands in the 227-231 nm regions [42], as already mentioned for GO, due to $\pi \rightarrow \pi^*$ transitions (Fig. 2a). UV-DR spectrum of modified graphene oxide in the range of 200-400 nm demonstrated that melamine had a maximum absorption at 240 nm (Fig. 2b). This peak was assigned by Hirt and Salley to $\pi\pi^*$ transition, a transition that is symmetry-forbidden in melamine [48]. Dewar and Paoloni argued that absorption at 240 nm is due to an electronically forbidden, but vibrationally allowed [49]. Kammer investigated electronic properties of melamine using UV-vis spectra and showed the absorption spectrum of melamine [50]. For modified graphene oxide (Mel-GO), the peak at 235 nm was observed confirming that Mel was present in Mel-GO (Fig. 2c). The UV-DR spectrum of PMoV illustrated absorption bands at 250 and 306 nm, which are related to octahedral coordinated Mo^{6+} , and arise because of the Mo–O and V–O charge-transfer absorptions in the skeleton of Keggin type polyoxometalate (Fig. 2d). These two absorption bands appeared in the UV-DR spectrum of catalyst with a shift due to immobilization of PMoV on the surface of modified graphene oxide. In the supported catalyst, the peaks in 244 nm and 303 nm could be related to Keggin type polyoxometalate (Fig. 2e). Hence, the results are indicative of the fact that primary Keggin type structure has been immobilized on the surface of modified graphene oxide showing a strong interaction with catalyst. Fig. 2f showed the overlay of all samples confirming that the Keggin type polyoxometalate immobilized on the surface of modified graphene oxide.

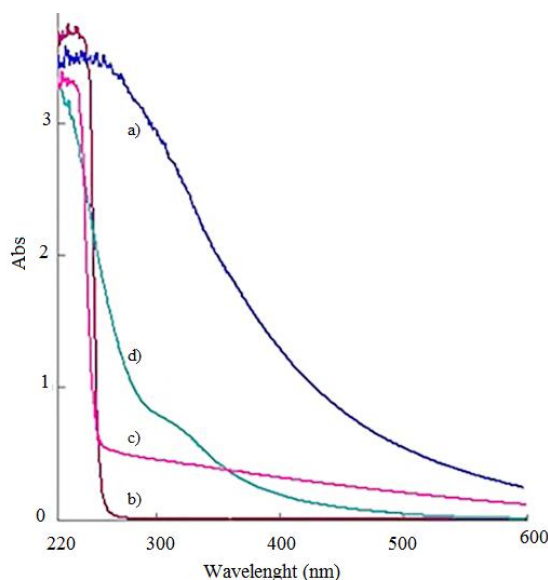


Figure 2. UV-DR spectra of a) GO, b) melamine, c) Mel-GO, d) PMoV- Mel-GO

To investigate the effect of the modification procedure on the surface morphology, surface FESEM images were prepared, and then they were compared together in Fig. 3. The FESEM images of GO are also shown in Fig. 3a where the morphology of GO showed layers with about 24 nm thickness. The morphology of Mel-GO is directly observed in the FESEM images of Fig. 3b. The surface morphologies of Mel-GO and GO are the same by observation, and both kinds of materials have wrinkled layers. It is proved that Mel-GO kept the 2D structure as GO. Fig. 3c shows that the surface

morphology was changed by supporting the PMoV, confirming that Keggin type polyoxometalate was immobilized on the surface of modified graphene oxide. The morphologies and nanostructures of the nanoparticles were approximately spherical. If we assume a nanoparticle spherical, the average diameters of nanoparticles are estimated to be 13 nm to 17 nm regions by averaging their diameters when they are measured in different directions in the FESEM images. This result shows the immobilization of Keggin type polyoxometalate on the surface of modified graphene oxide.

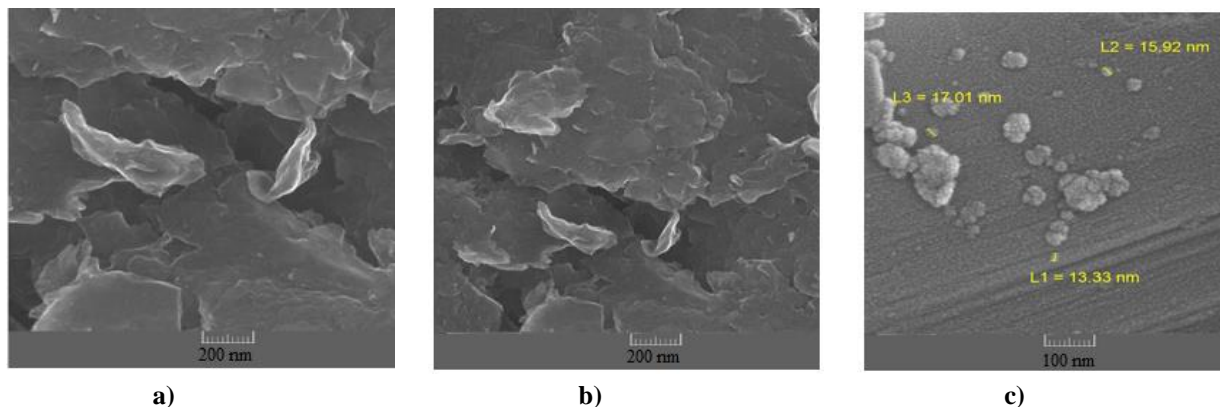


Figure 3. FESEM images of a) GO, b) GO-Mel, c) PMoV@ Mel-GO

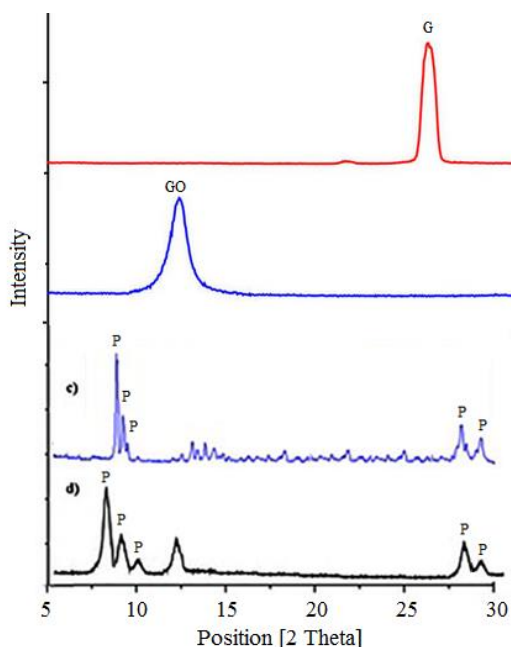


Figure 4. XRD images of a) Graphite, b) GO, c) PMoV, d) PMoV@ Mel-GO, G: Graphite, GO: graphene oxide, P: polyoxometalate

Fig. 4 shows XRD patterns of graphite, GO, PMoV and PMoV@ Mel-GO. The peak related to graphite structure, shown in Fig 4a, shows the peak corresponding to graphite [51] at $2\theta = 26.5^\circ$. The two-theta position of the (001) GO diffraction peak shows a range of $2\theta = 7-12^\circ$ (Cu K_α radiation)

based on the quantity of residual water intercalated between basal planes in a GO film (Fig. 4b) [42]. The peaks related to Polyoxometalate skeleton were observed at $2\theta = 28.1$ and 28.8 and below $2\theta = 10$ at $2\theta = 8.2, 8.9, 9.2$ and 9.2 [44] (Fig. 4c). Fig 4c shows XRD pattern of PMoV, the peaks corresponding to polyoxometalate skeleton were observed at $2\theta = 8.2, 8.9, 9.2, 28.2$ and 28.9 two-theta. Immobilization of Keggin type polyoxometalate (PMoV) on the surface of GO-Mel led to a change in the powder XRD pattern when compared with that for GO-Mel, confirming the formation of a new material compared to Mel-GO pattern, and a possible change in crystallinity and interplanar space [45]. The supporting procedure led to the disappearance of the smoother and more compressed surface than that of intact polymer. In addition, XRD patterns show absence of any impurities in the prepared sample. D parameter, defined as crystallite size of the catalyst sample, was calculated according to Scherer's equation Eq. (1):

$$D = 0.9\lambda/\beta \cos\theta \quad \text{Eq. (1)}$$

In the mentioned formula, λ and β refer to the wavelength of X-ray and full width at half maximum of the peak at diffracting angle θ , respectively. For the supported catalyst, the average diameters of particles were estimated to be 13 nm by averaging their diameters when they were measured in different directions in the FESEM images (Fig. 4d).

3.2. Electrochemical cyclic voltammetry

To study the electrochemical behavior of the POM that is supported on Mel-GO, which can not be dissolved in water, a three dimensional bulk modified carbon paste electrode (CPE) was fabricated by using the supported catalyst. This electrode was prepared by mixing the graphite powder as the conductive material, supported POM as the electro-active species, and silicon oil as the pasting liquid. The electrochemical studies were carried out in 0.2 M HCl aqueous solution because POM is unstable in neutral and basic aqueous solutions. Fig. 5 shows the cyclic voltammograms in 0.2 M HCl aqueous solution at a bare CPE, and CPE modified with POM – Mel@GO. It can be seen from Fig. 5 that in the potential range of -1 to 2 V (vs. Ag/AgCl), there is no redox peak at the bare CPE, while some consecutive redox processes are observed at the modified CPE. The above experimental results showed that POM can be supported on the surface of modified GO. According to Fig. 5, curves a and b represent the CVs of polyoxometalate and supported catalyst, respectively. At the modified electrode, there is an intensified anodic peak at the same potential, showing that Polyoxometalate nanoparticles are effective in improving the electrochemical behavior of modified electron. In fact, the supported catalyst/CPE caused about 2.0-fold increase in oxidation peaks compared to Polyoxometal/CPE. This behavior is due to both fascinating electron transfer and increasing active surface area. Moreover, the higher background current at supported catalyst/CPE also certified that the real surface area of modified electrode has been increased. It should be noted that electron-transfer rate of supported catalyst should be faster than polyoxometalate [52]. The above results clearly reveal that POM–Mel@GO demonstrates significantly enhanced electrochemical performance compared to intact POM. The relatively good capacitive performance of the POM–Mel@GO is due to the presence of grafted melamine, which can have a high concentration of surface functional groups for linkage of

polyoxometalate that can increase the electroactive surface area for double-layer charge storage, and good dispersion of POM on the surface of Mel@GO. Thus, it increases the accessibility of the available active sites in the supported catalyst.

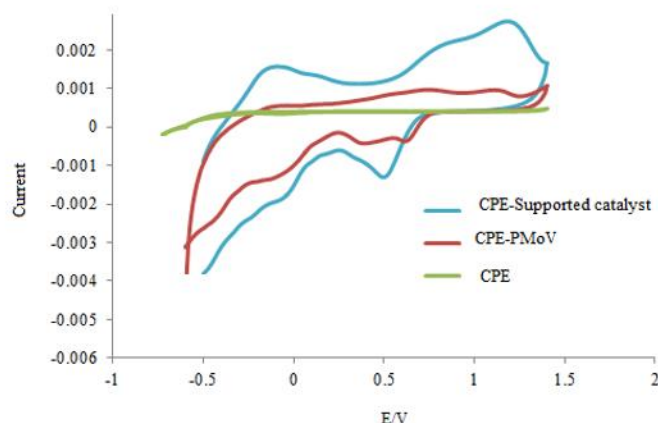


Figure 5. Cyclic voltammograms of samples, 50 mV/s scan rate: The concentration of each species is 1.0×10^{-3} M.

The electroactive surface areas of the pure CPE and catalyst/CPE were obtained by CV technique in the range of -1 to 2 V for 1.0 mM $K_3Fe(CN)_6$ as a probe in 0.1 M HCl. The slope of I_p vs. $v^{1/2}$ curve was determined by varying the scan rate from 0.01 to 0.15 V/s; and the electroactive surface area was obtained from the Randles-Sevcik equation for a reversible process [53] from equation (2).

$$I_{pa} = 2.69 \times 10^5 n^{3/2} A C_0 D_R^{1/2} v^{1/2} \quad \text{Eq. (2)}$$

Where I_{pa} denotes the anodic peak current (A), n represents the electron number, A refers to the surface area of the electrode (cm^2), D_R defines the diffusion coefficient ($cm^2 s^{-1}$), C_0 shows the concentration of $K_3Fe(CN)_6$, and v is the scan rate $V s^{-1}$. The electroactive surface area for supported catalyst modified electrode, it was approximately greater than that for CPE pure.

3.3. Electrochemical impedance spectroscopy

Electrochemical impedance spectroscopy (EIS) was applied to analyze the electronic conductivity changes at surface chemically modified electrodes. The Nyquist diagram contains a semicircle diameter at high frequencies, which is showed the electron-transfer resistance (R_{et}), and a linear portion at low frequencies might be appoints to diffusion process [53].

Electrochemical impedance spectroscopy is a powerful technique to investigate the interfacial properties of modified electrodes. During the deposition of charged PMoV, the electrical properties of the support are changed. The capacitance, the film resistance, the charge transfer resistance at the interface and the surface charge will be changed during the supporting procedure. In order to study the effect of the polyoxometalate structure on the overall electrochemical properties of the supporting procedure, electrochemical impedance spectroscopic experiments were performed after adsorption of PMoV. Fig. 6 shows the results of electrochemical impedance spectroscopy studies on multilayer electrodes with bare electrode, and supported catalyst immobilized on the surface of bare electrode

when $[\text{Fe}(\text{CN})_6]^{3-/4-}$ is used as the redox probe. The Nyquist diagram contains a semicircle diameter at high frequencies, which shows the electron-transfer resistance (R_{ct}), and that a linear portion at low frequencies might be attributed to diffusion process. Fig. 6 shows the Nyquist plots of the bare CPE (a), and supported catalyst/CPE (b). The equivalent circuit shown in Fig. 6, containing the circuit, consists of R_s as the solution resistance, W as the Warburg impedance, Q standing for the constant phase element, and R_{ct} referring to the charge transfer resistance [53]. The R_{ct} value of PMoV-CPE decreased remarkably, and it was attributed to the supreme conducting properties of the PMoV through facilitation electron transfer and increased surface area. As discussed above, the immobilization procedure and interaction between the polyoxometalate and the surface of the modified graphene oxide play a significant role in the charge transfer process [54].

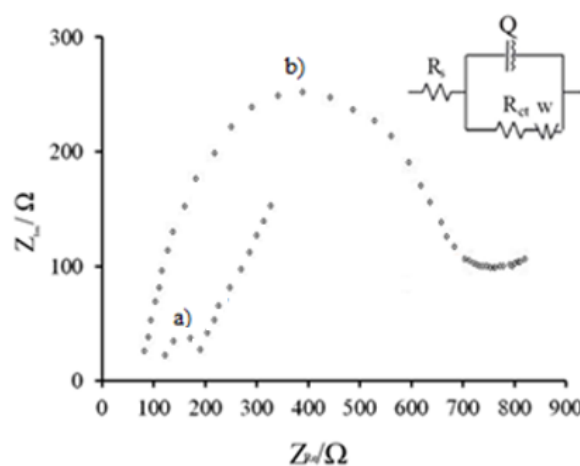


Figure 6. (A) Nyquist plot for the electrochemical impedance measurements in the presence of $3\text{mM}[\text{Fe}(\text{CN})_6]^{4-/3-}$ redox probe at sputtered Au electrodes terminated with (a) supported catalyst/CPE, (b) CPE, Conditions: polarization potential: 0.15 V, frequency: 5.0×10^{-3} to 10^5 Hz

3.4. Photocatalytic activity of supported catalyst in degradation of MB

Methylene blue was selected as the model dye for considering photocatalytic degradation of dyes as pollutants. These dyes had absorption in the visible region at 663 nm in water. The photocatalytic reaction was performed under different experimental conditions using different amounts of catalyst, various pH, and different intensities of ultrasonic irradiation in constant initial concentration of methylene blue for considering photocatalytic reactions. This was done without irradiation, and the pH conditions were changed from acidic to basic. The results showed that the optimized pH was 6.1. Methylene blue, as a selected dye, had absorption in the visible region at 663 nm in water. For investigating the effect of catalyst amount on the photocatalytic activity in degradation of methylene blue, it was found that the optimum amount of the catalyst for photocatalytic degradation of methylene blue was around 17.5 mg of the synthesized catalyst, which was made for the degradation of methylene blue solution, as displayed in 3D surface images. The rate of dye degradation was increased by enhancing the amount of catalyst, which could be due to the increase in its exposed surface area. However, it must be noted that after a certain limit (17.5 mg), if the amount of

catalyst had been increased further, there would have been a saturation point. The amount of Photocatalyst has an effect on the number of active sites on photocatalyst as well as on the penetration of light through the suspension. Increase in loading the Photocatalyst can enhance the rate of deactivating the activated molecules by striking the ground state Photocatalyst.

The effect of initial dye concentration on removal was investigated. The CCD equation of actual factors was solved by partial differential calculus for obtaining the optimum values of A, B and C. The optimized value is shown below, and the optimized data were obtained for this study: A (time) = 66 min, B (catalyst amount) = 17.5 mg, and C (pH) = 6.1. It should be noted that all the experiments were carried out for constant initial concentration of methylene blue (20 ppm). Theoretical R (% degradation) = 98.9%, and experimental R (% degradation) was 97.71 % obtained at optimized conditions.

Table 1. Constraints applied for optimization process obtained from CCD experiments

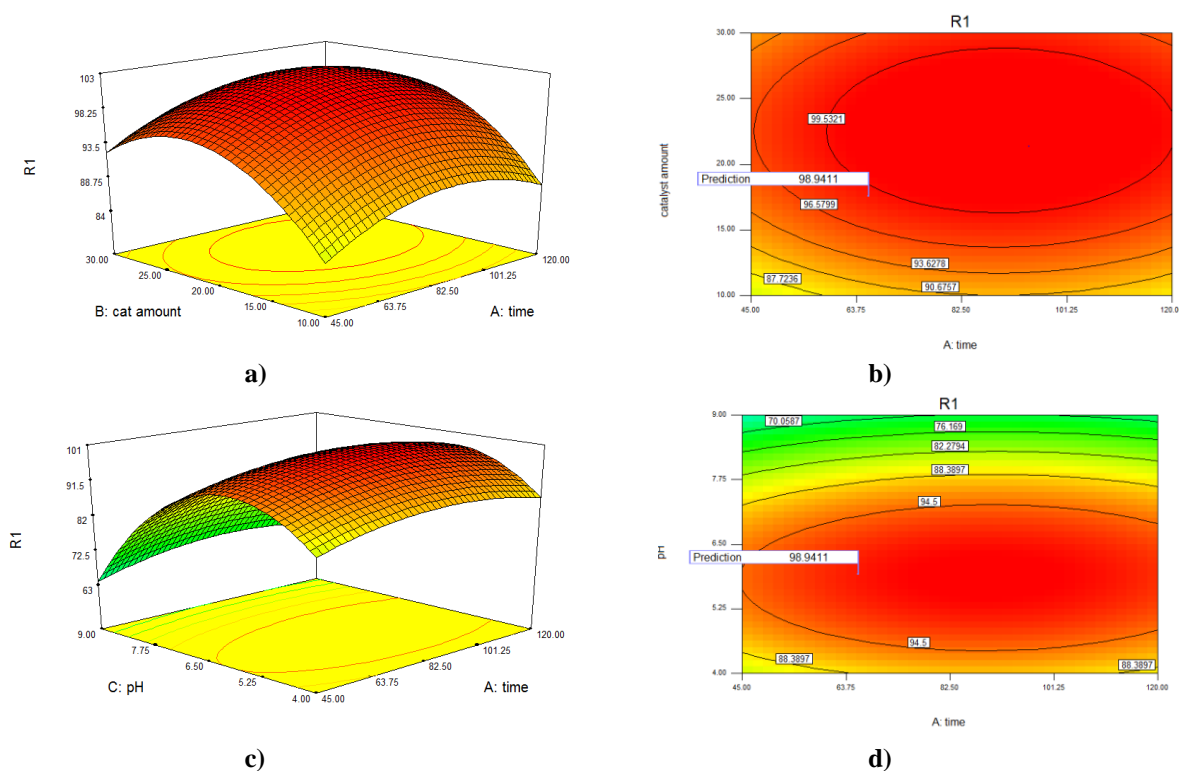
Catalyst amount	Time	pH	Removal%
17.5 mg	66 min	6.1	97.71%

In order to analyze the regression of the obtained data and to estimate the coefficient of the regression equation, design expert 7.0.0 software was used. The equations were validated by statistical tests called the ANOVA, to determine the significance of each term in the equations fitted, and to estimate the goodness of fit in each case. To determine the individual and cumulative effects of these variables and the mutual interactions between them, we drew response surfaces for the experimental results that were obtained from the effect of different variables on the percentage removal of dye. The model summary statistics results are shown in Table 2. The small values of coefficient of variation (C. V. %) of 0.89 and standard deviation (Std. Dev.) of 0.61 showed the reliability. The smaller anticipated residual sum of squares (PRESS) of 21.81 is a criterion of how good the model fits each point in it. The smaller the PRESS statistics, the better the model fits the data points. The above results indicate that the proposed quadratic model guarantees a precise demonstration of the experimental data as well as the high validity and adequacy of the model in predicting the degradation percentage of methylene blue. The Fisher's F value with a low probability ($p < 0.0001$) showed that the model was significant. The multiple correlation coefficient (R^2) demonstrated the goodness of the model. Moreover, R^2 value is 0.992, which could be explained by the developed quadratic model, and the predicted R^2 values were in agreement with adjusted R^2 , which means all the terms depicted in the model were significant. In this case, the non-significant lack-of-fit (0.09) confirmed that the quadratic model was valid for this process.

Table 2. The model summary statistics results obtained from design expert 7.0.0 software

Std. dev.	Mean	C.V. %	PRESS	R-squared	Adjusted R-squared	Predicted R-squared	Adeq precision
0.61	78.32	0.89	21.81	0.992	0.972	0.893	79.23

Interpretation of the pH effects on the efficiency of dye photo-degradation process is very difficult because it has multiple roles, and it is related to the ionization state of the surface according to the following reactions, and to that of reactant dyes and products like acids and amines. pH changes can thus influence the adsorption of dye molecules onto the modified graphene oxide surfaces; an important step for the photocatalytic oxidation to take place. Usually, the wastewater from textile industries has many different pH values. Generally, pH has a vital role in the characteristics of textile wastes and in the generation of hydroxyl radicals. Hence, attempts have been made to study the influence of pH in the degradation of dyes. The effect of different levels of initial solution of pH and time on dye degradation using the Keggin type polyoxometalate supported on modified GO can be predicted from the contour plot as shown in Fig.7. From the contour plot, it can be observed that dye degradation percentage increased with an increase in time and pH. Solution of pH affects the chemistry of the degradation of dyes, the activity of pH on the adsorbent surface, and competition in degradation of dyes for the binding sites [16]. The optimized pH and contact time were 6.1, 66 min. The combined effect of adsorbent dosage and contact time of removal dye were shown in the contour plot of Fig. 7. The percentage of dye removal increased with an increase in adsorbent dosage. Higher adsorbent dosage enhanced the catalytic active sites force and increased the dye adsorption. From the results, it was observed that an actual removal efficiency of 97.71% was achieved at 17.5 mg catalyst amount and 66 min of contact time. The combined effect of adsorbent dosage and pH on dye removal was shown in the contour plot of Fig. 7. Higher adsorbent dosage enhanced the catalytic active sites force and increased the dye adsorption. From the results, it was observed that an actual removal efficiency of 97.71% was achieved at optimized pH, and the catalyst amounts were 6.1 and 17.5 mg. Overall, the important degree of the test based on the slopes in graphs in Fig. 6 on conversion was: pH > catalyst amount > time.



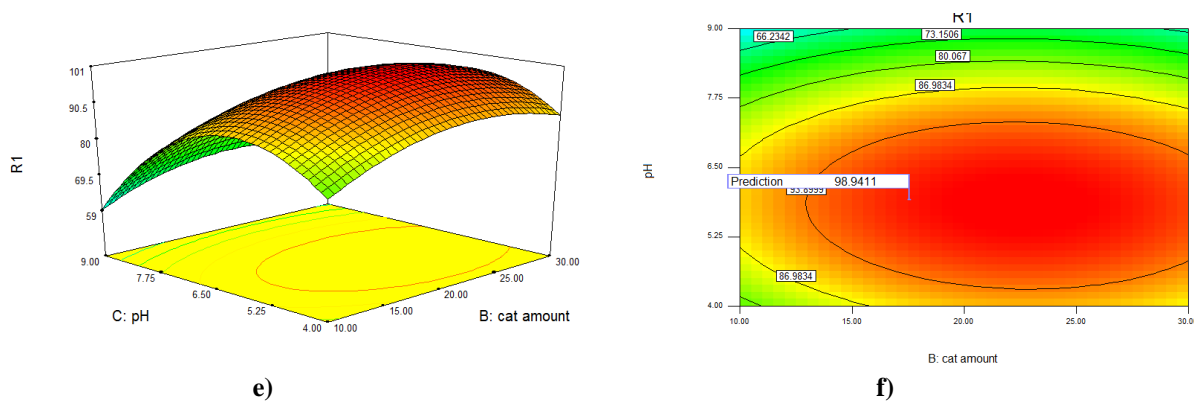


Figure 7. Three dimensional response surface graph and counter plots for the degradation of dye wastewater (a) % dye degradation versus time (min) and catalyst amount (mg); (b) counter plots for time and catalyst amount; (c) % dye degradation versus pH and time; (d) counter plots for pH and time; e) % dye degradation versus pH and catalyst amount; and f) counter plots for pH and catalyst amount

In Fig. 8, we showed the regression plot of the trained network. That in Fig. 7 gave a correlation coefficient of 0.992. The high correlation coefficient of this plot illustrated the reliability of the neural model with the experimental data.

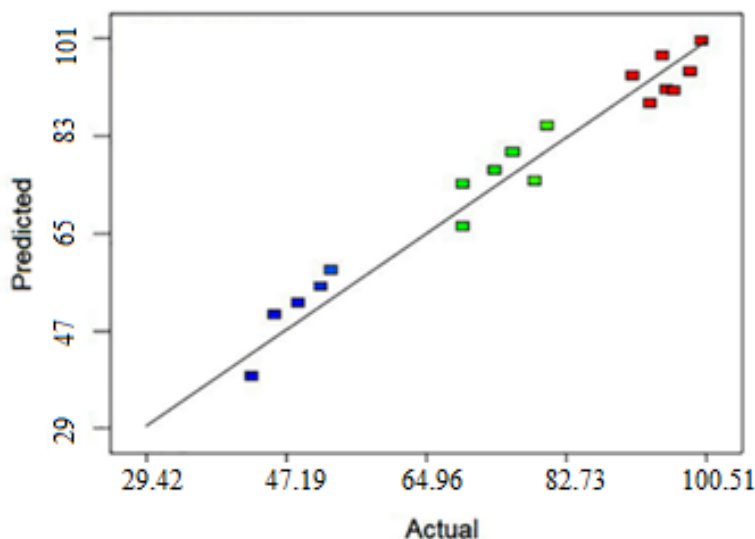


Figure 8. Regression plot (actual vs. predicted) using three input variables

To consider the effect of supported polyoxometalate on degradation of dyes, experiments were performed with polyoxometalate and melamine as catalyst in the same conditions. The result showed that even up to 90 minutes, the degradation of methylene blue was a trace in the presence of melamine and PMoV as catalyst (Fig. 9a, Fig 9b). Therefore, the influence of supporting procedure on photocatalytic degradation of methylene blue was obvious.

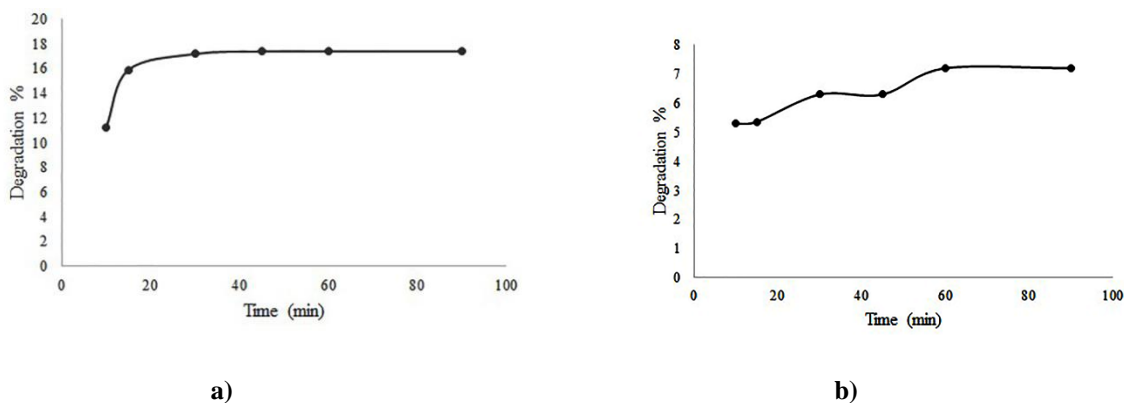


Figure 9. a) Degradation of methylene blue with PMoV as catalyst in the same condition,
 c) Degradation of methylene blue with melamine as catalyst in the same conditions, sample amount: 17.5 mg, temperature: 25 °C, time: 66 min, pH=6.1

3.5. Catalytic behavior, separation, and recyclability of supported catalyst in degradation of MB

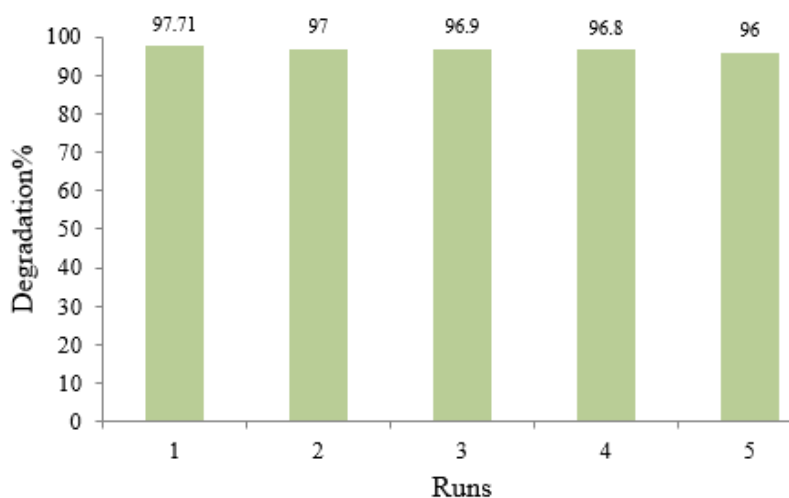


Figure 10. Reusability of catalyst in degradation of MB with synthesized catalyst; for the first cycle, the conditions were catalyst amount 17.5 mg, pH= 6.1, reaction time 66 min

The stability of the supported catalyst was monitored by using multiple sequential degradation of dyes with synthesized catalyst under visible light. For each of the repeated reactions, the catalyst was recovered, washed thoroughly with water and dried before being used with fresh methylene blue solution. Fig. 10 shows that the catalysts were consecutively reused five times. They were recovered for four runs without any loss of activity. The investigation of the catalysts was intact after photocatalytic reaction, the FT-IR spectrum of catalysts, after being reused, was taken. The result illustrated that the peaks corresponding to the supported catalyst were shown at 773 cm^{-1} , 840 cm^{-1} , 1050 cm^{-1} and 1620 corresponding to Mo=O, O-Mo-O, P-O and C=C groups, respectively, with a shift due to adsorption procedure (Fig. 11).

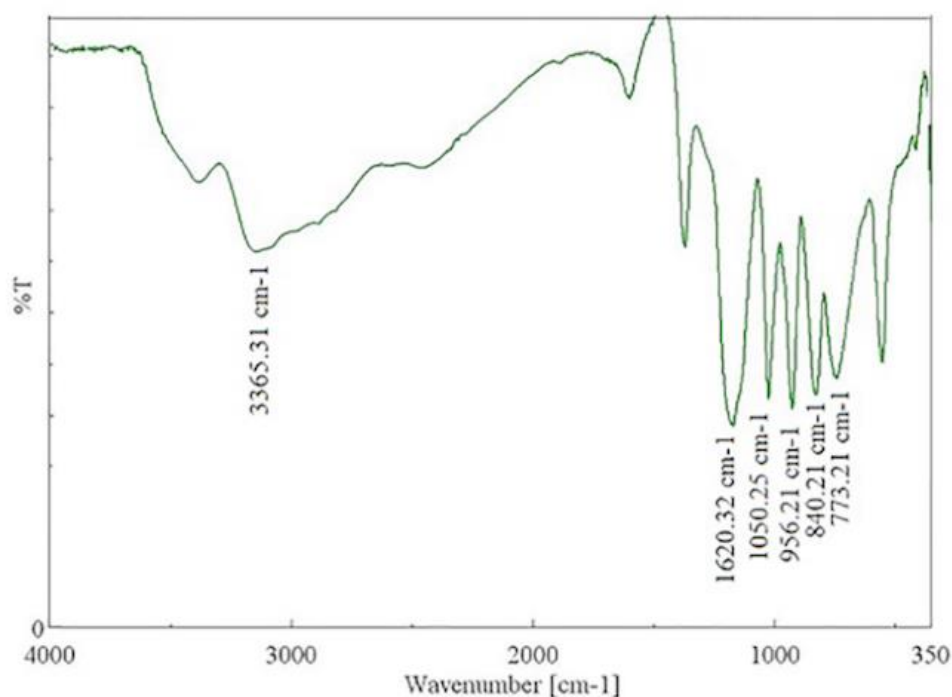


Figure 11. FT-IR spectrum of reused catalysts after degradation of methylene blue

3.6. Proposed mechanism for degradation of MB under visible light

Many investigators have proposed various mechanisms for the degradation of dyes as pollutants. To expose to visible light irradiation, the metal ions were excited by light so that they could give excited electrons. An electron will be provided in the conduction band by this excited state, and a hole is left in the valance band. Then, this electron is trapped by molecular O_2 , and it forms O_2^- ions. The hole in the valance band creates hydroxyl radical from hydroxyl ions; and this can readily attack the adsorbed dye, resulting in their complete mineralization [55]. Comparison between the photocatalytic activity of the supported catalyst and those of other reported catalysts for the degradation of dyes is listed in table 3.

Table 3. Comparison between reaction data for the present method in degradation of dyes and other reported methods

Catalyst	dyes	Ref
PMoV@Mel-GO	Methylene blue	This work
CuO@GO	Methyl orange	56
Ag ₃ PO ₄ @GO	Methylene blue	57
TiO ₂ @rGO	Organic dyes	58
TiO ₂ @GO	Methylene blue	59
Fe ₃ O ₄ @rGO@TiO ₂	Organic dyes	60

3.7. Catalytic activity of supported catalyst in oxidation of DBT

Optimization of the conditions for the oxidation of solid DBT was performed with formal batch method. In this study, acetonitrile was used as the solvent for the oxidative desulfurization of the product. Due to its low boiling point, it was suitable for the separation of product. The DBT was not oxidized at room temperature; hence, the effect of the O/S molar ratio (Fig. 13) and catalyst loading (Fig. 12) on DBT oxidation was investigated at 50°C. The results showed that when we used 0.05 g of catalyst and a 3:1 O/S molar ratio for 90 min, we produced the corresponding sulfone (DBTO₂) with 100% selectivity.

To consider the influence of the catalyst amount on oxidation of DBT and to have the highest DBT conversion at minimum amount of catalyst, a series of experiments with differing amounts of catalysts was used. The results shown in Fig. 12 indicated that the percentage of the conversion of DBT was increased by enhancing the amount of catalyst because higher catalyst amount could provide more active site for the catalytic desulfurization reaction. However, with further increase in catalyst amount from 0.01 g to 0.2 g, the catalytic activity was reduced. As reported by Li, this was due to the decrease in contact area between DBT and catalyst because of the saturation of active sites of catalyst [61].

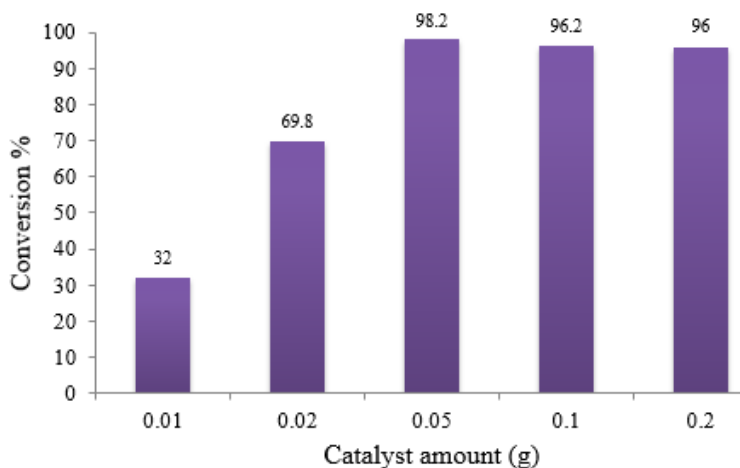
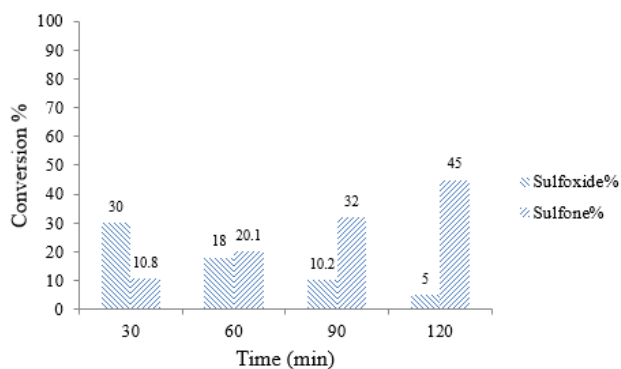


Figure 12. Effect of the catalyst amount on selective oxidation of DBT to DBTO₂ in the presence of supported catalyst at 50°C and O/S = 3:1, catalyst amount: x g, for 120 min



a)

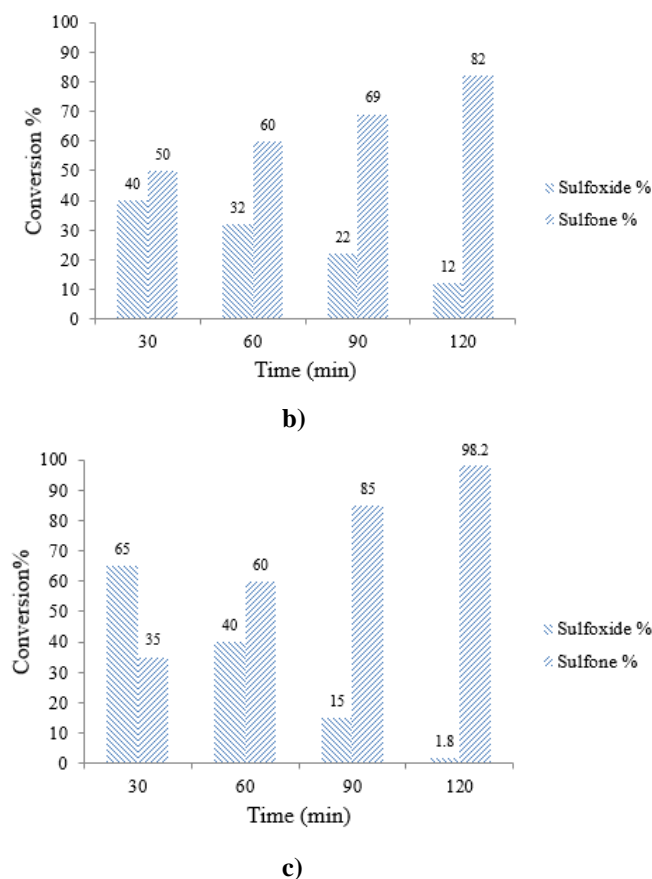


Figure 13. Effect of O/S molar ratio on the oxidation of DBT to DBTO₂ in the presence of supported catalyst (0.05 g) at 50 °C. (a) 1:1; (b) 2:1; (c) 3:1 for 120 min

The amount of catalyst used in this research was lower than that previously reported probably because good dispersion of polyoxometal on the surface of modified grapheme oxide increased the number of reactive sites. It was found that the optimum amount of the catalyst for catalytic oxidation of DBT was around 50 mg of the synthesized catalyst.

Mass analysis (Fig. 14) recorded M^+ at m/z 216 confirming that the sulfone of DBT was found. The intense m/z peaks of the obtained crystals were observed at 187, 168 and 160, which could be ascribed to $C_{11}H_7SO$, $C_{12}H_8O$ and $C_{10}H_8S$ ions moieties of DBTO₂, respectively [62]. An examination between FT-IR spectra of the formed crystal and DBT is shown in Fig. 15. The two compounds showed almost similar bands; however, in the spectrum of the mentioned crystal, we witnessed 2 new bands with strong intensities at 1286 and 1161 cm^{-1} , which could be related to the asymmetrical and symmetrical stretching vibration modes of $O \leftarrow S \rightarrow O$, respectively [62]. Hence, under the experimental conditions that were applied, the DBT compound was oxidized selectively to corresponding sulfone, and it was removed from the mixture by being adsorbed on the catalyst surface. In ¹H-NMR of DBT, the peaks in the range of 7-8 ppm assigned aromatic hydrogens of phenyl ring (Fig. 16). The conversion and percentages of each compound in the reaction mixtures were analyzed using gas chromatography (Fig. 17).

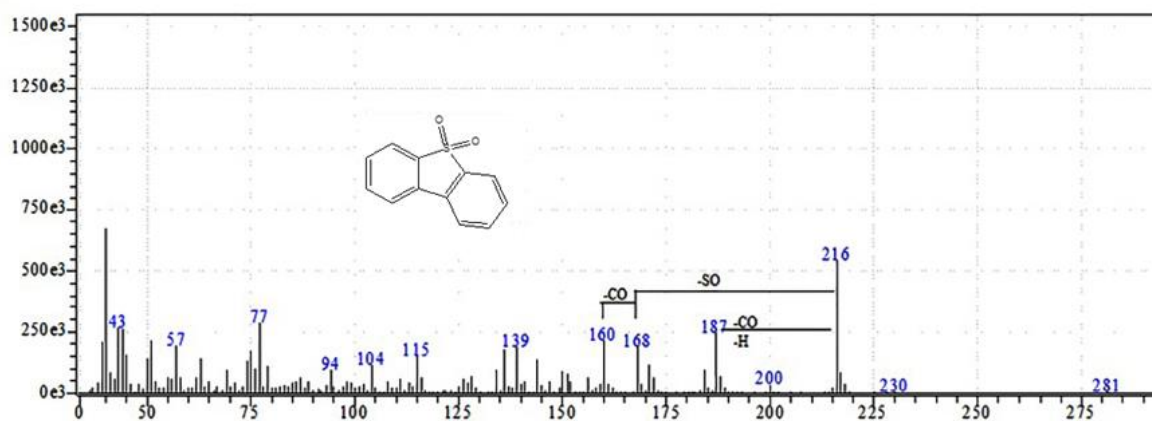


Figure 14. Mass spectrum of dibenzothiophene sulfone product

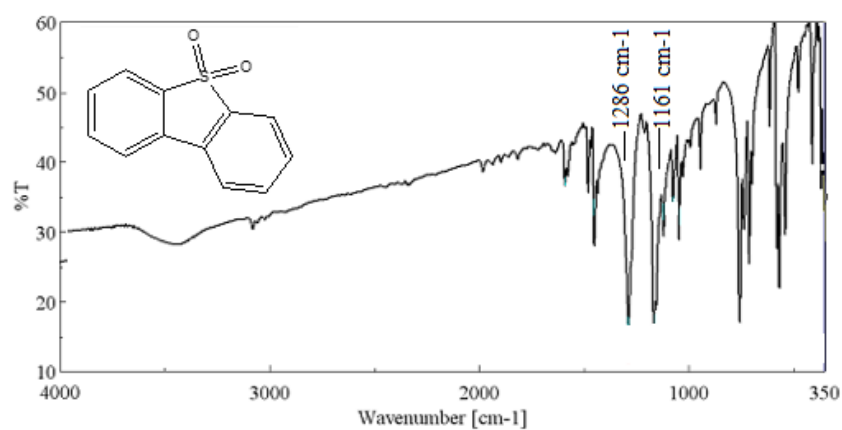


Figure 15. FT-IR spectrum of dibenzothiophene sulfone product

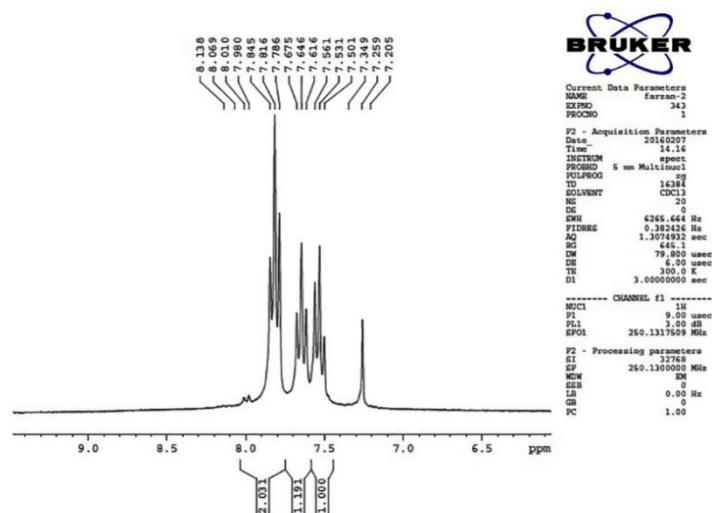


Figure 16. ^1H -NMR spectrum of dibenzothiophene sulfone

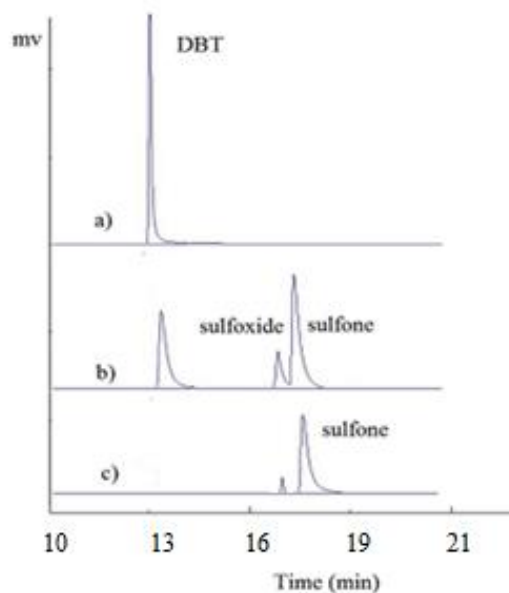
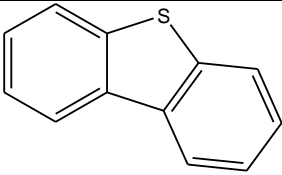
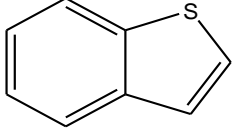
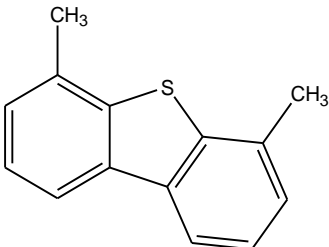


Figure 17. GC analysis of oxidation product

Table 4. Oxidation of sulfur compound to sulfone product with H_2O_2 catalyzed by synthesized catalyst GC yields based on the toluene as the internal standard

Entries	Sulfur compound	% Yield
1 DBT		98.2
2 BT		80.2
3 4,6-DMDBT		90.2

Temperature (50 °C), B: time (120 min), H_2O_2 / DBT3:1, 50 mg catalyst. Yield is determined using GC

To establish the general applicability of the process, various sulfur compounds were subjected to the oxidation system using the synthesized catalyst (Table 4, entries 1-3). The relativities of the sulfur compounds were influenced by two main factors, i.e., the electron density on the sulfur atom band and the steric hindrance of the sulfur compound. Compared to BT, DBT shows higher reactivity,

which can be explained by the higher electron density on sulfur atom of DBT. For DBT and 4,6-DMDBT, the difference in the electron density on the sulfur is very small. Therefore, the lower reactivity of 4,6-DMDBT is due to the steric hindrance of the methyl groups that limit the accessibility of the sulfur atoms to the catalytic active sites (Table 4).

Comparison of reaction data for the present method and other reported methods are listed in Table 5.

Table 5. Comparison of reaction data for the present method and other reported methods

Catalyst	Sulfur compound	Ref
POM@ Mel@GO	DBT	This work
POM@ Graphite carbon	DBT	63
Mixed metal oxide@ GO	DBT	64

4. CONCLUSIONS

Keggin type polyoxometalate-functionalized modified graphene oxide (denoted as PMoV@ Mel-GO) was prepared by anchoring PMoV on the surfaces of Mel-coated GO nano-sheets. The catalyst showed excellent photocatalytic activity in degradation of dyes under visible light and, therefore, could be reused at least four times with only a slight decrease in the catalytic activity. Electrochemical characterization showed that electron-transfer rate of supported catalyst should be faster than polyoxometalate. The results showed that modified graphene oxide could accelerate electron transfer in photocatalytic procedures due to its large surface area. In addition, the catalyst showed high activity and desired selectivity in the catalytic oxidation of dibenzothiophene to sulfone product. The heterogeneous catalyst could be readily separated using centrifugation from the oxidation system, and loss of activity was negligible when the catalyst was recovered in five consecutive runs.

ACKNOWLEDGEMENT

The authors are thankful to Payame Noor University in Isfahan Research Council; and contributions from Birjand University are greatly acknowledged.

References

1. S. Tangestaninejad, M. Moghadam, V. Mirkhani, I. Mohammadpoor and H. Salavati, *J. Iran. Chem. Soc.*, 7 (2010) 161.
2. M.T. Pope and A. Muller, *Angew. Chem. Int. Ed. Eng.*, 30 (1991) 34.
3. D. C. Duncan, T.L. Netzel and C.L. Hill, *Inorg. Chem.*, 34 (1995) 4640.
4. H. Salavati and H. Saedi, *Int. J. Electrochem. Sci.*, 10 (2015)4208.
5. G. Licini, V. Conte, A. Coletti, M. Mba and C. Zonta, *Coord. Chem. Rev.*, 255 (2011) 2345.

6. S. Tangestaninejad, M. Moghadam, V. Mirkhani, I. Mohammadpoor-Baltork and H. Salavati, *J. Iran. Chem. Soc.*, 7 (2010) 161.
7. T. Ito, K. Inumaru and M. Misono, *Chem. Mater.*, 13 (2001) 824.
8. P. Lei, C. Chen and J. Yang, *Environ. Sci. Technol.*, 39 (2005) 8466.
9. X. Wang, Z. Chang, H. Lin, A. Tian, G. Liu, J. Zhang and D. Liu, *RSC. Adv.*, 5 (2015) 14020.
10. G. Xue, J. Xiong, H. Guo, G. Cao, S. Nie and H. Hu, *Electrochim. Acta*, 69 (2012) 315.
11. J. Xiong, W. Zhu, W. Ding, L. Yang, M. Zhang, W. Jiang and Z. Zhao, *RSC.*, 5 (2015) 16847.
12. J. Xiong, W. Zhu, H. Li, Y. Xu, W. Jiang, S. Xun, H. Liu and Z. Zhao, *AIChE J.*, 59 (2013) 4696.
13. C. Soldano, A. Mahmood and E. Dujardin, *Carbon*, 48 (2010) 2127.
14. T. Kuila, S. Bose, A. K. Mishra and P. Khanra, *Prog. Mater. Sci.*, 57 (2012) 1061.
15. D. R. Dreyer and S. Park, *Chem. Soc. Rev.*, 39 (2010) 228.
16. O. C. Compton and S. T. Nguyen, *Small*, 6 (2010) 711.
17. N. Varghese, U. Mogera and A. Govindaraj, *Chem. Phys. Chem.*, 10 (2009) 206.
18. L. H. Tang, Y. Wang and Y. Liu, *ACS. Nano*, 5(2011) 3817.
19. W. Lv, M. Guo and M. H. Liang, *J. Mater. Chem.*, 20(2010) 6668.
20. T. Ferri and D. Frasca, *Angew. Chem. Int. Ed.*, 50 (2011) 7074.
21. Q. Su, S. P. Pang and V. Alijani, *Adv. Mater.*, 21 (2009) 3191.
22. Y. Zhu, S. Murali, W. Cai, X. Li and J.W. Suk, *Adv. Mater.*, 22 (2010) 3906.
23. H.C. Hsu and I. Shown, *Nanoscale*, 5 (2013) 262.
24. H. P. Mungse, S. Verma and N. Kumar, *J. Mater. Chem.*, 21 (2012) 5427.
25. D. R. Dreyer, H. P. Jia and A. D. Todd, *Org. Biomol. Chem.*, 9 (2011) 7292.
26. Z. Lin, G. Waller, Y. Liu, M. Liu and C. P. Wong, *Adv. Energy. Mater.*, 2 (2012) 884.
27. Z. Y. Lin, M. K. Song, Y. Ding, Y. Liu and M. L. Liu, *Phys. Chem. Chem. Phys.*, 14 (2012) 3381.
28. D. C. Wei, Y. Q. Liu, Y. Wang, H. L. Zhang, L. P. Huang and G. Yu, *Nano Lett.*, 9 (2009) 1752.
29. M. Heitzmann, L. Basaez, F. Brovelli, C. Bucher, D. Limosin, E. Pereira, B. L. Rivas, G. Royal, E. Saint-Aman and J. Moutet, *Electroanalysis*, 17 (2005) 1970.
30. F. T. Vasquez and P. B. Balbuena, *J. Phys. Chem. B*, 108 (2004) 15992.
31. Y. Xue, H. Chen, J. Qu and L. Dai, *2D Mater.*, 2 (2015) 044001.
32. A. B. Bourlinos, D. Gournis, D. Petridis, T. Szabo, A. Szeri and I. Dekany, *Langmuir*, 19 (2003) 6050.
33. B. Wang, B. Luo, M. Liang, A. Wang, J. Wang, Y. Fang, Y. Chang and L. Zhi, *Nanoscale*, 3 (2011) 5059.
34. Z. Sheng, L. Shao, J. Chen, W. Bao, F. Wang and X. Xia, *ACS. Nano*, 5 (2011) 4350.
35. M. Du, J. Sun, J. Chang, F. Yang, L. Shi and L. Gao, *RSC. Adv.*, 4 (2014) 42412.
36. Z. Lin, Y. Liu, M. Liu and C. Wong, *Carbon*, 53 (2013) 130.
37. Q. Wei, X. Tong, G. Zhang, J. Qiao, Q. Gong and S. Sun, *Catal.*, 5 (2015) 1574-1602.
38. H. Gao, L. Song, W. Guo, L. Huang, D. Yang, F. Wang, Y. Zuo, X. Fan, Z. Liu, W. Gao, R. Vajtai, K. Hackenberg and P. M. Ajayan, *Carbon*, 50 (2012) 4476.
39. X. Li, H. Wang, J. T. Robinson, H. Sanchez, G. Diankov and H. Dai, *J. Am. Chem. Soc.*, 131 (2009) 15939.
40. X. Tang, W. Li, Z. Yu, M. A. Rafiee, J. Rafiee, F. Yavari and N. Koratkar, *Carbon*, 49 (2011) 1258.
41. G. Liao, S. Chen, X. Quan, H. Yu and H. Zhao, *J. Mater. Chem.*, 22 (2012) 2721.
42. D. C. Marcano, *ACS nano* 4.8 (2010) 4806.
43. J. Zhang, Y. Tang, G. Li and C. Hu, *Appl. Catal. A: General*, 278 (2005) 251.
44. Z. Chen, J. Wang, F. Yu, Z. Zhang and X. Gao, *J. Mater. Chem. A*, 3 (2015) 11624.
45. Z. Jin, Q. Zhang, L. Hu, J. Chen, X. Cheng, Y. Zeng, Sh. Ruan and T. Ohno, *Appl. Catal. B: Environ.*, 205 (2017) 569.
46. B.V. Lotsch and W. Schnick, *Chem. Eur. J.*, 13 (2007) 4956.
47. E. Wirnhier, M.B. Mesch, J. Senker and W. Schnick, *Chem. Eur. J.*, 19 (2013) 2041.

48. R.C. Hirt and D.J. Salley, *J. Chem. Phys*, 21 (1953) 1181.
49. M.J.S. Dewar and L. Paoloni, *Trans. Faraday Soc*, 53 (1957) 261.
50. E. Kammer, Th. Dorfer, A. Csaki, W. Schumacher, P. DaCosta, N. Tarcea, W. Fritzsche, P. Rosch, M. Schmitt and J. Popp, *J. Phys. Chem. C*, 116 (2012) 6083.
51. 51.M. naebe, J. wang, A. amini, H. khayyam and N. hameed, *Scientific reports*, 4 (2014) 4375.
52. H. Salavati and H. Saedi, *Int. J. Electrochem. Sci*, 10 (2015) 4208.
53. A.J. Bard and L.R. Faulkner, *Wiley, New York* (1980).
54. Sh. Wang, L.Liu, W. Chen, E. Wang and Zh. Su, *Dalton Trans*, 42 (2013) 2691.
55. A. Ajmal, I. Majeed, R. Naseem Malik, H. Idrisc and M. Nadeem, *RSC. Adv*, 4 (2014) 37003.
56. S. Liu, J. Tian, L.Wang, Y. Luo and X. Sun, *Catal. Sci. Technol*, 2 (2012) 339.
57. G. Chen, M .Sun, Q .Wei, Y. Zhang and B.Zhu, *J. hazard. mater*, 244 (2013) 86.
58. L.M, Pastrana-Martínez, S. Morales-Torres, V. J. Likodimos, L. Figueiredo, J L Faria, P Falaras and A M. Silva, *Appl. Catal. B: Environ*, 123 (2012) 241.
59. S. P. Kim and H. C. Choi. *Bull. Korean. Chem. Soc*, 9 (2014) 2661.
60. X. Yang, W. Chen, J. Huang, Y. Zhou, Y. Zhu and C. Li, *Scientific reports*, (2015) 5.
61. Q N. Li, , Guang, H W. Jiang, Q. Hua, W. Ning, G Z. Qi, L. Qi, L H.Yu and Q Z. Yu, *Adv. Mat. Res*, 396 (2012) 827.
62. M.Chamack, A. R. Mahjoub and H. Aghayan, *Chem. Engin. Res. Design*, 94 (2015) 565.
63. W. Jiang , D. Zheng, S. Xun, Y. Qin, Q. Lu, W. Zhu and H. Li, *Fuel*, 190 (2017) 1.
64. R. Menzel, D. Iruretagoyena, Y. Wang and M. Mokhtar, *Fuel*, 181 (2016) 531.

© 2018 The Authors. Published by ESG (www.electrochemsci.org). This article is an open access article distributed under the terms and conditions of the Creative Commons Attribution license (<http://creativecommons.org/licenses/by/4.0/>).